December 1980

# Trends in the theory of atomic photoionization

Anthony F. Starace

*University of Nebraska-Lincoln*, astarace1@unl.edu

# Trends in the theory of atomic photoionization

Anthony F. Starace

**Abstract**

For VUV photon energies, detailed theoretical understanding of the photoionization process has been achieved for the case of a single electron ionized from one of the outer subshells of a closed-shell atom. This understanding is based qualitatively upon a few properties of realistic atomic central potentials and quantitatively upon a few distinct types of electronic interactions known generically as particle-hole interactions. Current theoretical research is mainly directed at understanding a broader class of atomic photoionization phenomena involving, e.g., open-shell atoms, electronic interactions not of the particle-hole class, real two-electron processes, and external electric and magnetic fields.

## I. Introduction

In the VUV-soft x-ray photon energy region, i.e., for photon energies in the 10-eV $\leq \hbar\omega < $ 1000-eV range, detailed theoretical understanding of the photoionization process has been achieved for the case of a single electron ionized from one of the outer subshells of a closed-shell atom. Qualitative aspects of this understanding are based upon a few properties of realistic atomic central potentials, which were used in the first attempts to interpret the experimental data obtained in the 1960s in this new photon energy region.[1] A more quantitative theoretical understanding of the new data, however, took much of the 1970s to develop, if we use the criterion that theoretically calculated results must agree with experimental measurements to within ~10%. Although a seemingly large number of competing theoretical methods were developed to treat atomic photoionization,[2] mainly of closed-shell atoms, these methods have in common the inclusion of certain key kinds of electronic interactions, known generically as particle-hole interactions. Thus one may summarize concisely our current understanding of closed-shell atom, single-electron photoionization processes by describing the effects of these important types of electronic interactions. Our aim in this paper is to present just such a concise summary of the physical basis for the successes of theory that have thus far been achieved. We discuss both the qualitative and the quantitative aspects of our current theoretical understanding. Furthermore we have attempted to outline the scope of current and future theoretical research by indicating those aspects of the photoionization process that either have not yet been fully explored or adequately understood. Due to the brevity of this paper, we have only been able to cite a relatively few references, chosen primarily for illustrative purposes. We refer the interested reader to other recent review articles for more detailed descriptions than can be presented here of the various theoretical[2] and experimental[3] methods and results.

## II. Realistic Central Potential Models

A. Qualitative Explanation of Nonhydrogenic Behaviors

The hydrogen atom cross section, which is nonzero at threshold and decreases monotonically with increasing photon energy, serves as a model for inner-shell photoionization cross sections in the x-ray photon energy range. For VUV photon energies, however, the cross sections for subshells with $l \geq 1$ frequently have the behavior shown in Figure 1 for the $4d$ subshell in Xe[4]: a cross section that rises from threshold to a maximum (the so-called delayed maximum above threshold) then decreases to a minimum (the so-called Cooper minimum[5]), then rises again to a second maximum, and finally decreases monotonically at high energies in accordance with hydrogenic behavior. The dominant channel contributing to the cross section in Figure 1 is that of the $f$ wave:

$$\text{Xe} 4d^{10}5s^2\,5p^6(^1\text{S}_0) + \gamma \rightarrow \text{Xe}^+ 4d^9 5s^2 5p^6 \epsilon f(^1P_1). \quad (1)$$
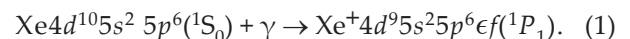
Using the realistic Herman-Skillman central potential[6] and adding to it the centrifugal potential $l(l+1)/2r^2$ for $l = 3$, one finds that the effective potential[7] (shown in Figure 2)
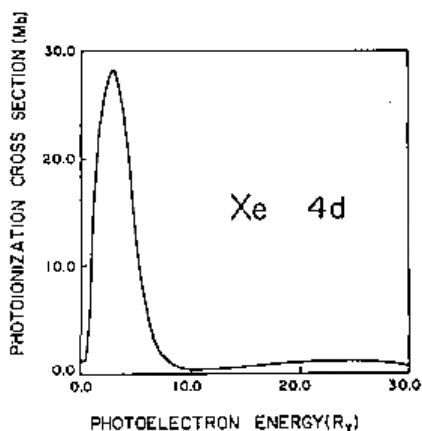
**Figure 1.** Theoretical photoionization cross section for the 4*d* subshell in Xe vs photoelectron energy. (Hartree-Fock-length results from Reference 4.)
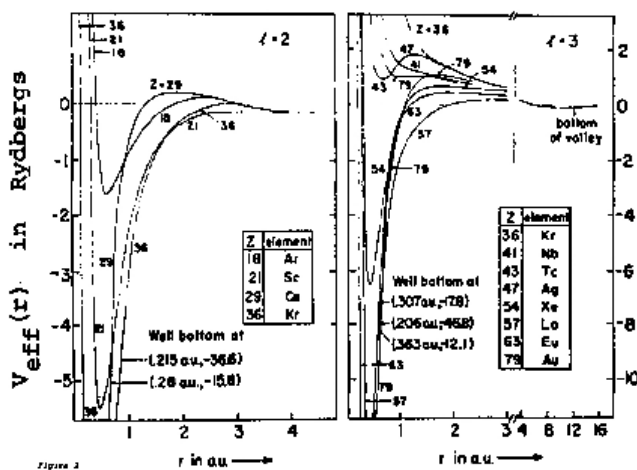


**Figure 2.** Effective potential $V_{eff}(r)$ plotted vs coordinate $r$ for $l = 2$ and $l = 3$ electrons. $V_{eff}(r)$ is the sum of the Herman-Skillman atomic potential $V(r)$ and the centrifugal potential $l(l + 1)/(2r^2)$ (from Reference 7).

that determines the radial continuum $f$ wave function has a potential barrier in Xe ($Z = 54$). This potential barrier prevents low-energy continuum $f$ electrons from penetrating the atomic core region (where the 4*d* electron is localized) until the continuum electron has sufficient energy to overcome the barrier. This is the explanation for the delayed cross-section maximum above threshold. Since the continuum $f$-electron wave function has a substantial amplitude only at large radial distances, the radial dipole amplitude $\langle 4d|r|\epsilon f \rangle$ is negative at threshold, since the outer loop of the 4*d* wave function has a negative amplitude. At large energies $\epsilon$, however, the dipole amplitude must have a hydrogenic behavior and hence must become positive. This implies that at some energy, usually occurring shortly after the continuum electron is able to surmount the potential barrier, the dipole amplitude is zero. This explains the occurrence of the Cooper minimum in the cross section. The second cross-section maximum is then just a result of the increase of the dipole amplitude to positive values before the hydrogen-like monotonically decreasing behavior begins.

The central potential model thus explains qualitatively the nonhydrogenic cross-section features observed experimentally for subshells with $l \geq 1$. Quantitatively, the central potential model cross sections disagree with experiment, often by factors of 2 near threshold. Furthermore the $s$-subshell cross sections cannot be interpreted at all. Thus the task of the 1970s for theoreticians was to discover which electronic interactions are responsible for the quantitative disagreement between central potential model predictions and experiment. Before discussing what was discovered, we emphasize the usefulness of the central potential model by mentioning two of its more recent contributions to the theory of photoionization.

### B. More Recent Results Obtained with the Central Potential Model

Experimental results on the 4*d*-subshell absorption spectrum in the rare earths[8] and the 3*p*-subshell absorption spectrum in the transition metals[9] have been interpreted largely on the basis of the central potential model.[10] These spectra are characterized by (1) an intense structured main peak above the 4*d* or 3*p* ionization threshold, which decreases in intensity with increasing atomic number $Z$, and (2) numerous weak resonance-like features in the vicinity of threshold. The main peak appears at first sight to be the above-described delayed maximum above threshold, particularly since, as shown in Figure 2, the $l = 3$ effective potentials in the rare earths ($Z = 57$ and $63$) and the $l = 2$ effective potentials in the transition metals (compare $Z = 29$) have significant potential barriers. However, the central potential model cross sections are very small and essentially flat! This puzzle was resolved when it was discovered that all the intensity in the central potential model goes into the discrete transition $4d \rightarrow 4f$ in the rare earths and $3p \rightarrow 3d$ in the transition metals,[10] as shown in Figure 3, which contrasts this behavior with that of the 4*d*-subshell cross section in Xe and the 3*p*-subshell cross section in Ar. The difference in behavior between Xe and the rare earths (respectively, Ar and the transition metals) is that in the former case the potential barrier keeps out all bound $f$ electrons (respectively, $d$ electrons), whereas in the latter case the potential well is deep enough to bind the 4*f* orbital (respectively, 3*d* orbital) in the inner-well region. The close proximity of the 4*f* and 4*d* orbitals in the rare earths and the 3*d* and 3*p* orbitals in the transition metals accounts for the large intensities observed in the following photoabsorption transitions:

rare earths: $4d^{10}4f^N + \gamma \rightarrow 4d^9 4f^{N+1}$,
transition metals: $3p^6 3d^N + \gamma \rightarrow 3p^5 3d^{N+1}$.    (2)
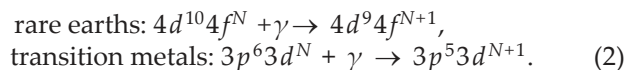
Calculations[11] of the term level structure of the configurations on the right in Equation (2) correspond in intensity and location with observed experimental features. The transitions in Equation (2) also explain why the observed main peak intensities decrease with increasing $Z$:
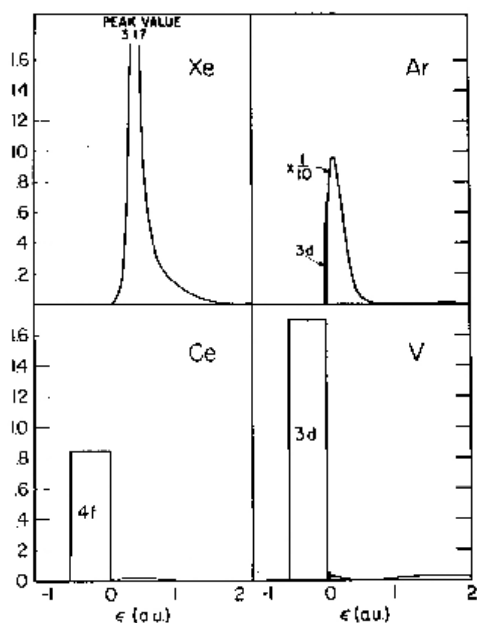
**Figure 3.** Squared radial dipole matrix elements $[\int_0^\infty P_{nl}(r)rP_{\epsilon l'}(r)dr]^2$, plotted as a function of $\epsilon$ using Herman-Skillman wave functions. For Ar and V, $nl = 3p$ and $l' = d$; for Xe and Ce, $nl = 4d$ and $l' = f$ (from Reference 10).
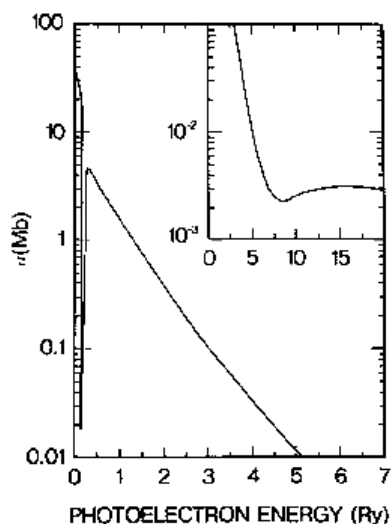


**Figure 4.** Photoionization cross section for the excited $5d$ orbital of Cs. Inset shows the high energy behavior of the cross section (from Reference 15).

The number of vacancies in the $4f$ or $3d$ subshells decreases with increasing Z. Although the decay of the excited configurations on the right in Equation (2) via autoionization,[10, 12] super Coster-Kronig[13] or other Auger transitions is still not well understood,[14] the central potential model prediction[10] that the absorption intensity passes through these configurations has been well confirmed and was the key to interpreting these very complex spectra.

Another recent prediction of the central potential model, not yet confirmed experimentally, is the occurrence of multiple minima in the photoionization cross section of excited atoms. In calculations for unexcited atoms, each subshell has been found to have at most a single Cooper minimum. Figure 4 shows the cross sections calculated for the $5d$ electron in excited Cs.[15] There is a sharp resonancelike feature just above threshold that is actually due to a change in sign of the $5d \rightarrow \epsilon f$ radial dipole matrix element from positive to negative. The usual Cooper minimum, in which there is a change in sign of this element from negative to positive, occurs at much higher energies (shown in the insert in Figure 4). The similarity of the first minimum to a window resonance indicates that one must be very careful in interpreting excited atom photoionization spectra.

## III. Quantitative Description of Closed-Shell Atom Single-Photoionization Spectra: The Particle-Hole Interactions

In the 1970s it was proved by a large number of calculations for closed-shell atoms that the most important electronic interactions are those in which two electrons interact in such a way as to either excite or de-excite each other out of or into their initial subshell locations in the unexcited atom. (When an electron is excited out of a subshell it is said to leave behind a vacancy or hole.) To analyze the effects of these interactions on the cross sections it is convenient to classify them in three categories, which we discuss in turn.

### A. Intrachannel Scattering Interactions

The many-body perturbation theory (MBPT) diagram for this interaction is shown on the left in Figure 5(a); on the right a slightly more pictorial description of this interaction is shown. The wiggly line indicates a photon, which is absorbed by the atom in such a way that an electron is excited out of the $nl$th subshell. During the escape of this excited electron, however, it collides or interacts with another electron from the same subshell in such a way that the second electron absorbs all the energy imparted to the atom by the photon; the first electron is de-excited back to its original location in the $nl$th subshell. For closed-shell atoms, the photoionization process leads to a $^1P_1$ final state in which the intrachannel interaction is strongly repulsive. Hence with respect to central potential model or average- of-configuration Hartree-Fock (HF) calculations, which include only a weaker average intrachannel interaction in generating the basis wave functions, inclusion of these interactions serves to shift the delayed maximum in the cross section to higher energies (usually too high) as well as to broaden this peak and decrease its amplitude. [Note that in those HF calculations (known as term-dependent HF calculations) that include the correct $^1P_1$ intrachannel interaction in solving for the HF wave functions, no further treatment of these interactions is necessary: one obtains cross sections equivalent to those obtained by starting from an arbitrary basis set of final state wave functions and explicitly treating the intrachannel interactions within this basis set.]
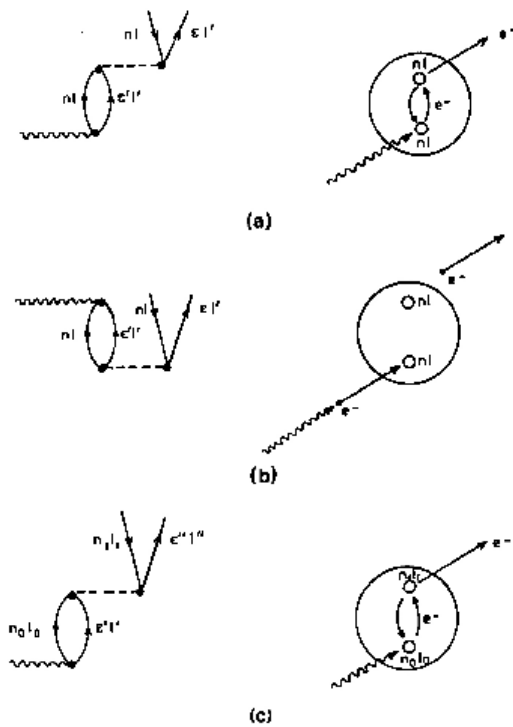
**Figure 5.** MBPT diagrams (left) and scattering pictures (right) for the following interactions: (a) intrachannel scattering following photoabsorption; (b) photoabsorption by a virtual doubly-excited state of the atom; (c) interchannel scattering following photoabsorption.
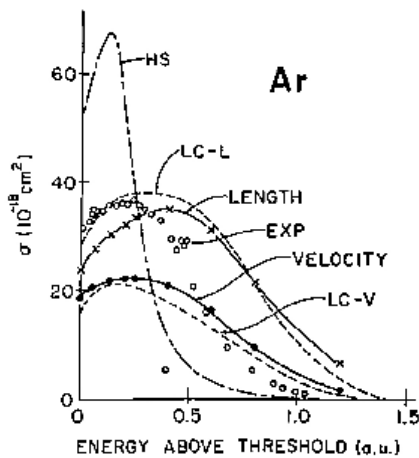


**Figure 6.** Photoionization cross sections for the 3p subshell of Ar: – · –, Herman-Skillman central potential model calculation; ——, intrachannel calculation of Starace[16]; - - -, close-coupling calculation of Lipsky and Cooper; ○, experimental results of Samson[17] (from Reference 16).

As an example of the effect of intrachannel interactions, consider the 3p-subshell photoionization cross section in Ar shown in Figure 6. The central-potential model calculation[16] (HS) has the same qualitative features as the experimental data[17] (open circles) but has a cross section that peaks at too low an energy and is far too high and narrow. The solid lines indicate the result of treating the intrachannel interactions within the basis of the central-potential model wave functions.[16] The result using the length form of the dipole matrix element

peaks at too high an energy due to the too repulsive intrachannel interaction. The result using the velocity form of the dipole matrix element gives too low a cross section, again due to the too repulsive intrachannel interaction that keeps the continuum wave function out of the small *r* region, which is weighted more strongly by the velocity dipole operator. The dashed curves represent close coupling calculations,[18] which include not only the intrachannel interactions but also certain weak interchannel interactions (discussed below) involving the 3s subshell. Clearly the results are not very different from the intrachannel calculations,[16] indicating another cause for the discrepancy with experiment.

### B. Virtual Double Excitations

The MBPT diagram for this type of interaction is shown on the left in Figure 5(b). Topologically this diagram is similar to that on the left in Figure 5(a). In fact, the radial parts of the two matrix elements are identical; only the angular factors differ. A more pictorial description of this interaction is shown on the right of Figure 5(b): The ground state of the atom before photoabsorption is shown to have two electrons virtually excited out of the *nl*th subshell. In absorbing the photon, one of these electrons is de-excited to its original location in the *nl*th subshell, while the other electron is ionized. These virtual double excitations imply a more diffuse atom than in central-potential or HF models with the effect that the overly repulsive intrachannel interactions are weakened, leading to cross sections that are in very good agreement with experiment. Recent calculations of Chang[19] for the Ar 3p- subshell cross section (Figure 7) demonstrate the effect of including these virtual double excitations. The curves labeled *I* are the length and velocity results including only the intrachannel interactions. Curves *II* indicate the effect of including virtual double excitations in the initial state: the length and velocity curves are in



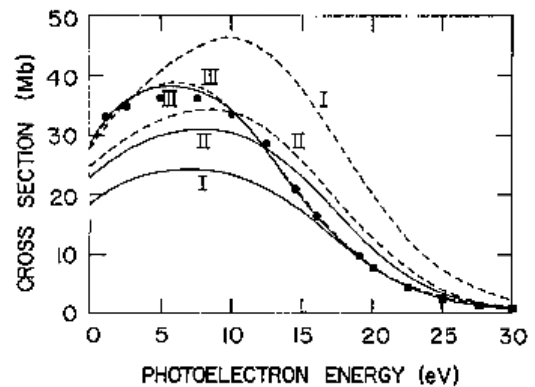**Figure 7.** Theoretical calculations of Chang[19] for the photoionization cross section of the 3p subshell of Ar. Dashed and solid lines give length and velocity results, respectively, in three levels of approximation discussed in the text. Experimentally measured values of the Ar cross section are indicated by the solid circles[17] and by the solid squares (Samson, unpublished) (from Reference 19).
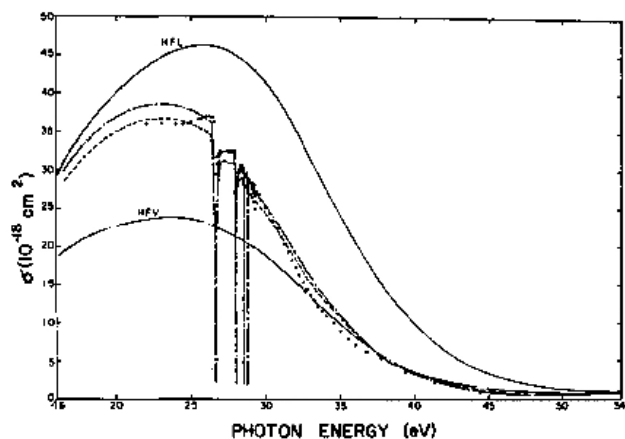
**Figure 8.** Photoionization cross section for the $3p$ and $3s$ subshells of Ar. HFL and HFV indicate the length and velocity results obtained using HF orbitals calculated in a $^1P_1$ potential. Dot-dash and dashed lines represent the length and velocity results of the MBPT calculation of Kelly and Simons.[20] Only the four lowest $3s \rightarrow np$ resonances are shown; the series converges to the $3s$ threshold at 29.24 eV. Experimental results are those of Samson[17] above 37 eV and of Madden *et al.*[21] below 37 eV (from Reference 20).
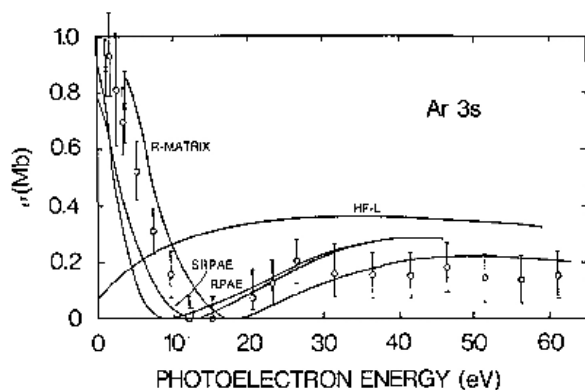


**Figure 9.** Photoionization cross section for the $3s$ subshell of Ar: $R$-Matrix, $R$-matrix (length) calculation of Burke and Taylor[22]; RPAE, RPA calculation of Amusia et al.[23]; SRPAE, simplified RPA calculation of Lin[24]; HF-L, Hartree-Fock (length) calculation of Kennedy and Manson[4]; ×, experimental data of Samson and Gardner[25]; ○, experimental data of Houlgate *et al.*[26] (from Houlgate *et al.*[26]).

better agreement, but there is still a sizable discrepancy with the experimental results[17] (solid circles). Finally curves *III* indicate the result of including virtual double excitations in both the initial and the ionic state. Now the length and velocity curves are virtually identical and are both in excellent agreement with experiment.

## C. Interchannel Interactions

A last type of particle-hole interaction that has been found to be important, particularly for $s$ subshells, is the interchannel interaction shown in Figure 5(c). This interaction has the same form as the intrachannel interaction shown in Figure 5(a), except now when an electron is photoexcited out of the $n_0l_0$th subshell, it collides or interacts with an electron in a different subshell—the $n_1l_1$th subshell—in such a way that the second electron is ionized, and the first electron falls back into its orig-

inal location in the $n_0l_0$th subshell. There are two major effects of this interaction: (1) when the binding energy of the $n_0l_0$th subshell is greater than that of the $n_1l_1$th subshell, discrete members of the $n_0l_0$th subshell channels show up as resonances in the $n_1l_1$th subshell cross section; (2) when the dipole amplitude for ionization of the $n_1l_1$th subshell is small compared with that for the $n_0l_0$th, for example, when $n_1l_1$ is an $s$ subshell, the zero-order $n_1l_1$th subshell cross section can be strongly modified by interchannel interactions.

As an example of the first effect—resonance behavior—we consider once again the photoionization of the $3p$ subshell in Ar, this time including also the effect of interchannel interaction with the $3s$ subshell. The channels under consideration are thus
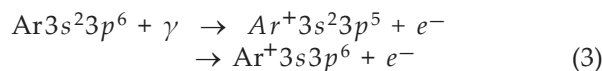
$$\begin{aligned} Ar3s^23p^6 + \gamma \ &\rightarrow \ Ar^+3s^23p^5 + e^- \\ &\rightarrow Ar^+3s3p^6 + e^- \end{aligned} \quad (3)$$

Figure 8 shows the MBPT calculation of Kelly and Simons,[20] which includes both intrachannel and interchannel interactions as well as the effect of virtual double excitations. The cross section is in excellent agreement with experiment,[17, 21] even to the extent of describing the resonance behavior due to discrete members of the $3s \rightarrow \epsilon p$ channel.

As an example of the second effect, strong modification of a weak dipole amplitude, we consider again the two channels in Equation (3), but this time we focus on the $3s$-subshell cross section. Figure 9 shows three calculations, which include intrachannel and interchannel interactions as well as virtual double excitations. There are the $R$-matrix calculation of Burke and Taylor,[22] the random phase approximation (RPA) calculation of Amusia *et al.*,[23] and the simplified RPA calculation of Lin.[24] As compared with the HF calculation[4] shown, which only includes the intrachannel interactions, these three other calculations show that interchannel interactions introduce a strong interference between the channels in Equation (3). This interference causes a minimum in the $3s$-subshell cross section in agreement with experiment.[25, 26]

As a final example of particularly strong interchannel interactions, we consider the $5s$-subshell cross section in Xe as influenced by the neighboring $4d$ and $5p$ subshells. The relevant channels are

$$\begin{aligned} Xe4d^{10}5s^25p^6 + \gamma \ &\rightarrow Xe^+4d^95s^25p^6 + e^- \\ &\rightarrow Xe^+4d^{10}5s5p^6 + e^- \\ &\rightarrow Xe^+4d^{10}5s^25p^5 + e^- \ . \end{aligned} \quad (4)$$
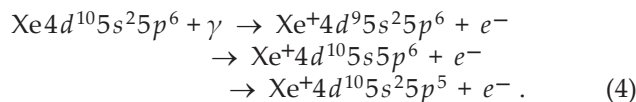
Figure 10 shows the calculations of Amusia and Cherepkov[27] in three approximations. The dot-dash line represents the HF result for the $5s$-subshell cross section. No interchannel interactions are included. The dashed line represents an RPA calculation including interchannel interaction with the $4d \rightarrow \epsilon f$ channel. One sees that the large delayed maximum in the $4d$-subshell cross section (compare Figure 1) is mirrored in the $5s$-subshell cross

**Figure 10.** Theoretical calculations of Amusia and Cherepkov[27] for the photoionization cross section of the 5$s$ subshell of Xe, showing the influence of interchannel interactions (see text for description of curves) (from Reference 27).
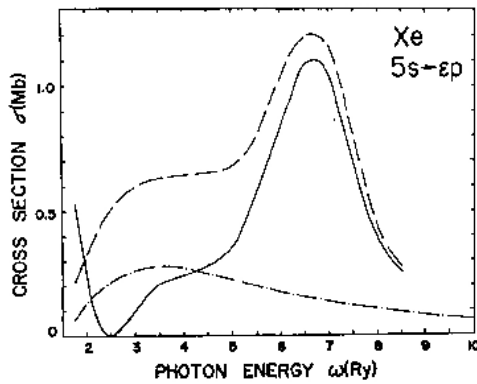
section. The solid line represents an RPA calculation including interchannel interaction with both the $4d \rightarrow \epsilon f$ and the $5p \rightarrow \epsilon d$ channels. One sees that interchannel interaction with the outer 5$p$ subshell produces interference leading to a zero in the 5$s$-subshell cross section.

### D. Remarks

The three types of interactions discussed are the most important for the outer $l \geq 1$ subshells of the rare gases and probably for all closed-shell atoms. These interactions form the essential physical content of the many *ab initio* theoretical methods that have been developed to treat atomic photoionization such as the RPA,[27, 28] the MBPT,[29] $R$-matrix method,[22, 30] the transition matrix approach,[19, 31] and the multiconfiguration HF approach[32] among others. We emphasize, however, that except for the RPA these methods are not restricted to treating only the particle-hole class of interactions. In particular, $s$ subshells have such small cross sections that other types of interaction may have a significant influence on them.[27] Some of these other interactions are mentioned in Sec. V.

## IV. Semianalytic Treatment of Resonance Phenomena

Resonances may be treated in an *ab initio* theoretical calculation by including the interchannel interactions described in the previous section. However, to describe the rapid oscillations in the cross section in a resonance region, one normally must perform many calculations over a very finely spaced set of energies. Fortunately this is usually not necessary, since much of the rapid energy variation of the cross section near a resonance can be described analytically, thus reducing significantly the number of numerical calculations. We describe briefly below the two main methods for treating isolated and Rydberg series of resonances.

### A. Isolated Resonances: Fano Profile Formula

Fano[33] has shown that for a single resonance interacting with a single continuum channel, the cross section in the neighborhood of the resonance may be described in terms of three parameters, which may be obtained either by fitting to experimental data or by an *ab initio* theoretical calculation. These parameters are the resonance energy $E_{res}$, the resonance width $\Gamma$, and the so-called $q$ parameter, which is equal to $\pi$ times the ratio of the direct photoabsorption amplitude (in which a ground state electron is photoexcited directly to the resonance state) and the indirect photoabsorption amplitude (in which a ground state electron is photoexcited to the continuum and is then scattered into the resonance state). In terms of these parameters, the cross section $\sigma(E)$ as a function of energy $E$ in the neighborhood of the resonance is given by

$$\sigma(E) = \sigma_0 \, (q + \epsilon)^2/(1 + \epsilon^2) \qquad (5a)$$

where

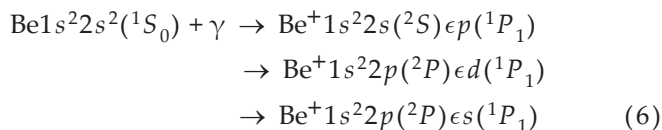$$\epsilon = (E - E_{res})/(1/2\Gamma). \qquad (5b)$$

For $|q| > 1$, one observes primarily a resonance peak, whereas for $|q| < 1$, one observes primarily a resonance window. Fano has also treated the cases of several discrete states interacting with a continuum channel and of a single discrete state interacting with several continua.[33] Similar formulas have been obtained for partial cross sections,[34] branching ratios,[34] and $\beta$ parameters[35] in the neighborhood of a resonance.

### B. Rydberg Series of Resonances: Quantum Defect Theory

Just below an excited ionic state threshold, one is faced with the seemingly hopeless task of describing the infinite Rydberg series of resonances converging to this threshold. The quantum defect theory (QDT) of Seaton[36] and of Lu and Fano[37] permits an analytic treatment of the resonance energy behavior using only the following two assumptions: (1) For radii $r > r_0$, where $r_0$ is of the order of the atomic radius, a photoelectron is assumed to move only under the influence of a pure Coulomb attraction. Hence the photoelectron wave function for $r > r_0$ may be written as a linear combination of regular and irregular Coulomb functions, which are analytically known. The coefficients of this linear combination are determined by matching conditions at the radius $r = r_0$ and thus contain all dynamical information of the photoabsorption process. (2) The matching coefficients are assumed to be slowly varying functions of energy near threshold since they are determined in the region $r < r_0$, where the atomic potential is very deep. That is, small variations of the photoelectron's asymptotic kinetic energy are not significant compared with the instantaneous kinetic energy in the region $r < r_0$. One may obtain these matching coefficients by *ab initio* calculations at one or at most a few energies,[36, 38] or by fitting to experimental energy level and oscillator strength data.[37]

As a striking example of the usefulness of the QDT, consider the calculation of Dubau and Wells[39] on the

photoionization of Be shown in Figure 11. Three channels were considered:

$$Be1s^22s^2(^1S_0) + \gamma \rightarrow Be^+1s^22s(^2S)\epsilon p(^1P_1)$$
$$\rightarrow Be^+1s^22p(^2P)\epsilon d(^1P_1)$$
$$\rightarrow Be^+1s^22p(^2P)\epsilon s(^1P_1) \quad (6)$$

The first channel belongs to the lower 2s threshold, and the other two channels belong to the upper 2p threshold. The solid line in Figure 11 connects the results of a completely *ab initio* close-coupling calculation [which includes intrachannel and interchannel interactions among the channels in Equation(6)], which was necessarily performed on the finely spaced energy mesh indicated by the dots. Coincident with the close-coupling calculation, except far from the threshold on the left-hand side of the figure, is the result of a QDT calculation, which is shown by a dashed line whenever it deviates significantly from the close-coupling result. The QDT result is obtained using a few dynamical parameters calculated above the 2p threshold by the close-coupling method and then simply extrapolating these parameters below threshold. While the extrapolation breaks down a few electron volts below threshold (i.e., near the spurious 2p2d resonance), the power of the QDT is clearly demonstrated. The pluses in the figure show the QDT result for the cross section averaged over the autoionizing resonances just below threshold. This average is seen to join smoothly onto the cross section above threshold, in agreement with theorems of Baz[40] and Gailitis.[41]

## V. Current Research

Up to now we have presented only what is firmly established in the theory of atomic photoionization through the comparison of alternative calculational methods with well-determined experimental results. It is of course more difficult to give an assessment of those areas of photoionization research in which theory and experiment disagree, or in which there are few experimental measurements, or in which theoretical advances are very recent. For these reasons we only comment briefly in what follows on a number of current research areas, which, taken together, indicate the breadth of this field and its relevance to atomic physics as a whole.

### A. Real Two-Electron Processes

The importance of virtual two-electron excitations on single photoionization processes has been discussed in Section III. Here we discuss real two-electron processes in which, following photoabsorption, two electrons are either ionized or excited out of the atomic ground state.

#### 1. Double Photoionization

In contrast to single-electron photoionization, it is not known theoretically what asymptotic boundary condition to apply to the final state wave function in the
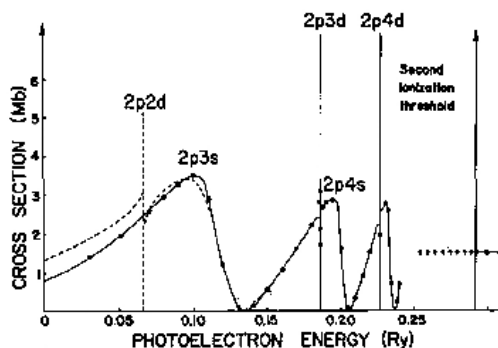


**Figure 11.** Theoretical calculations of Dubau and Wells[39] for photoionization of Be: ●, results of a close coupling calculation whose trend is indicated by the solid line; - - -, results of a QDT extrapolation of the close-coupling results from above the 2p ionization threshold. Note that the 2p2d resonance is spurious and may be eliminated by alternative QDT extrapolation techniques; +, cross section averaged over autoionizing resonances (from Reference 39).

case of two-electron photoionization. In simplest terms, it is not known how the two ejected electrons screen one another, particularly when they emerge from the same subshell. In the case of complete screening they see a net Coulomb charge of +1, while in the case of no screening they see a net Coulomb charge of +2; reality lies between. This important asymptotic problem has recently been examined by Altick,[42] who obtains asymptotic forms for two-electron wave functions. No calculations using the forms have yet been carried out. Below we review the available detailed calculations using more standard methods.

*1. Two electrons ejected from an outer subshell.* Helium is the prototype system for studying correlations of two electrons. Yet, at present, experimental measurements[43] of the double-to-single ionization ratio in He, $\sigma^{2+}/\sigma^+$, are -50% higher than the best available theoretical calculations,[44, 45] which use a correlated wave function in the initial state and a symmetrized product of uncorrelated Coulomb wave functions in the final state. While final state correlations are thus not treated, these calculations do demonstrate the importance of initial state correlation: when the correlated initial state wave functions are replaced by HF wave functions the calculated ratio $\sigma^{2+}/\sigma^+$ decreases by ~80% ! [44]

More detailed information regarding the influence of various physical processes on the double-ionization cross section has been provided by MBPT calculations. The first such calculation for Ne by Chang *et al.*[46] found the double-to-single ionization cross-section ratio, $Ne^{++}2p^4$: $Ne^+2p^5$, to be 11.1% at a photon energy of 278 eV. This result is in excellent agreement with Carlson's[47] measured value of 11 ± 1%. The calculation shows that the final state processes designated as core rearrangement and virtual Auger transition are just as important as initial state correlations in producing double ionization.

The energy dependence of the Ne double-photoionization cross section has been calculated by Chang and Poe,[48] again using MBPT, over the energy range from threshold to 220 eV above. Excellent agreement with ex-

periment[43, 47, 49] is achieved near threshold and at high energies, but near the cross-section maximum the calculated results are considerably higher than experiment, as shown in Figure 12. This calculation also shows that at low photon energies all energy distributions among the two electrons are nearly equally probable, but at high photon energies it is much more probable for one electron to take nearly all the available kinetic energy and for the other to have very little. The MBPT calculation of Carter and Kelly[50] is also shown in Figure 12. For $\hbar\omega > 120$ eV their results are in excellent agreement with experiment, but for lower photon energies their results disagree with both experiment and the calculations of Chang and Poe.

The double-photoionization cross section for argon over an energy range from threshold to ≈200 eV above has been calculated by Carter and Kelly.[51] Near threshold and at higher energies their results are in excellent agreement with experiment.[43, 47, 49] Near the peak in the experimental cross section, however, their results lie 20% lower than experiment and are shifted to higher energies. These calculations show that second-order perturbations lower the dipole length cross sections significantly, particularly near the cross-section peak (where this lowering amounts to ≈15%), but have only a small effect on the dipole velocity cross sections. Carter and Kelly[52] have also calculated the double-photoionization cross section of carbon, which represents the first such study for an open-shell atom.

We conclude that the MBPT calculations have identified some important final state correlations which, in addition to initial state correlations, contribute to double photoionization. At high photon energies, where one electron is moving much faster than the other, the MBPT cross sections are in very good agreement with experiment. Near the peak in the experimental cross sections in Ne
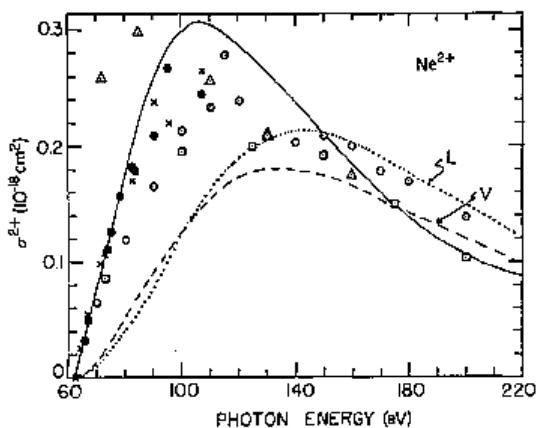


**Figure 12.** Double-photoionization cross section of Ne as a function of photon energy: ——, theoretical calculations of Chang and Poe[48] using the dipole velocity formula; - - -, ·····, theoretical calculations of Carter and Kelly[50] using the dipole velocity $V$ and dipole length $L$ formulas; △, experimental measurements of Carlson[47]; ●, experimental measurements of Samson and Haddad[49]; ×, experimental measurements of Samson and Kemeny (unpublished); □, experimental measurements of Schmidt *et al.*[43]; ○, experimental measurements of Wight and Van der Wiel.[43]
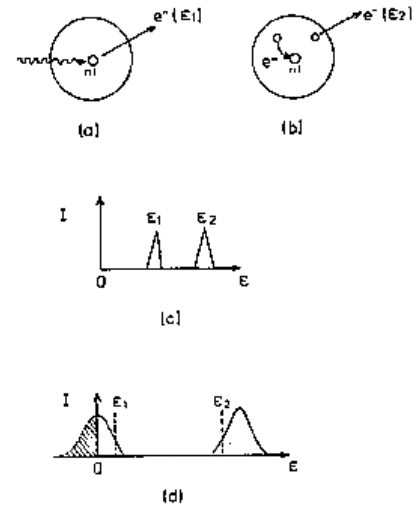


**Figure 13.** Effect of PCI in Auger decay following inner-shell photoionization: **(a)** pictorial description of inner-shell photoionization producing an electron with kinetic energy $\epsilon_1$; **(b)** pictorial description of Auger decay producing an electron with kinetic energy $\epsilon_2$; **(c)** electron energy distribution when $\epsilon_1 \gg 0$ (no PCI); **(d)** electron energy distribution when $\epsilon_1 \gtrsim 0$ (PCI shifts peak of electron 1 to lower energies and shifts peak of electron 2 to higher energies).

and in Ar, however, the MBPT cross sections differ significantly from the experimental results. At threshold, two[48, 51] of the three MBPT calculations for Ne and Ar are in excellent agreement with experiment.

*2. Two electrons ejected from an inner and outer subshell.* For very high photon energies in which an inner-shell electron is ejected very rapidly from an atom, the subsequent ejection of a second electron may be regarded as due to the relaxation of the excited ion. Theoretical calculations employing such a sudden or shake-off approximation[53] work well at high photon energies, even though they ignore final state interactions. When the photoelectron leaves slowly, however, one observes the so-called post-collision-interaction (PCI) effect[54] on the electron energy distributions. Figure 13(a) shows pictorially the initial inner-shell photoionization, followed by [Figure 13(b)] the ejection of a second electron due to an Auger transition. In Figure 13(c) the photoelectron energy distribution is shown in the case where $\epsilon_1 \gg 0$, so that the Auger decay occurs long after the escape of the first electron. The effect of PCI is seen in the energy distributions in Figure 13(d), where $\epsilon_1 \gtrsim 0$, and thus the Auger decay occurs while the first electron is escaping. Final state interactions are very important in this latter case. In simple terms, the first electron experiences a stronger net ionic charge after the Auger decay and is thus slowed down or even trapped in a Rydberg level. The Auger electron, on the other hand, experiences a weaker net ionic charge due to partial screening by the first electron and thus leaves faster. The semiclassical analysis of PCI by Niehaus predicts electron energy distributions that are in very good agreement with experiment.[54] No quantum mechanical description of PCI has yet been given.

## 2. Photoionization Plus Excitation

In one respect this process is simpler than double photoionization: since only a single electron is ionized, the final state wave function satisfies well-determined asymptotic boundary conditions. However, one must still deal with the multiplicity of excitation channels and their mutual interaction. Even for the simple process

$$\text{He} + \gamma \;\rightarrow\; (\text{He}^+)^*(n = 2) + e^-, \qquad (7)$$
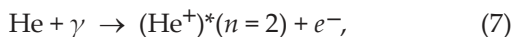
a close-coupling calculation including even $n = 3$ channels[55] gives a cross section that is 30–50% higher than recent experimental data[56] over an energy range from 15 to 40 eV above the $n = 2$ threshold.

Regarding the transition in Equation (7) we note that only the so-called + final states are populated with any intensity.[57] Furthermore, Macek[58] has shown that in a hyperspherical coordinate description, the + states emerge simply as one of the adiabatic final states. In hyperspherical coordinates the six electron coordinates $\mathbf{r}_1$ and $\mathbf{r}_2$ are replaced by the set $R$, $\alpha$, $\hat{r}_1$, and $\hat{r}_2$, where

$$R = (\, r_1^2 + r_2^2 \,)^{1/2}, \qquad (8a)$$

$$\alpha = \arctan(r_2/r_1). \qquad (8b)$$

The adiabatic approximation assumes that the angular motion in $\alpha$, $\hat{r}_1$, and $\hat{r}_2$ proceeds much faster than the radial motion in $R$. Using only the lowest $^1S_0$ and $^1P_1$ initial and final adiabatic state wave functions in hyperspherical coordinates, Miller and Starace[59] calculated the photoionization cross section for He,

$$\text{He} + \gamma \;\rightarrow\; \text{He}^+(n = 1) + e^-, \qquad (9)$$
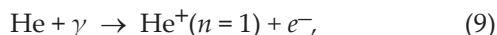
and obtained agreement with experiment[60] to within 1% at threshold, within 4% at 1 Ry above threshold, and within 12% at 1.9 Ry above threshold. Application of the hyperspherical coordinate method to the excitation process in (7) is in progress.[59] Note that similarly good results using this method have recently been obtained by Greene[61] for the Be-photoionization cross section below the Be$^+$(2p) threshold.

## B. Interactions Other than Those of the Particle-Hole Type

### 1. Relativistic Interactions

The relativistic RPA calculations of Johnson and co-workers[62–64] for the outer subshells of the rare gases represent a major advance of theory. Results for partial cross sections,[63] fine structure branching ratios,[63] photoelectron angular distributions,[63] and photoelectron spin polarizations[64] are all in very good agreement with experiment. As an example of the results obtained, consider those for the Xe 5s-subshell angular distribution asymmetry parameter $\beta$ shown in Figure 14. In the absence of relativistic interactions, only the $^1P$ channel $5s^2 \rightarrow 5s\epsilon p(^1P)$ is allowed and $\beta = 2$ independent of energy. Relativistic interactions permit also the forbidden $^3P$ channel $5s^2 \rightarrow 5s\epsilon p(^3P)$, and interference with the allowed $^1P$

channel causes $\beta$ to vary with energy. Not surprisingly, the largest variations in $\beta$ occur near the minimum in the 5s-subshell cross section, where the $^1P$ dipole amplitude is smallest. Figure 14 shows that the three fully relativistic calculations (i.e., the Dirac-Fock calculation of Ong and Manson[65] and the two relativistic RPA calculations of Johnson and Cheng[63]) all show $\beta$ to vary between 2 and 0. Only the relativistic RPA calculation including all interchannel interactions among the 4d, 5s, and 5p subshells, however, reproduces the experimental data.[66, 67]

The $K$-matrix calculation[68] shown in Figure 14 starts from a nonrelativistic basis of HF wave functions and only treats spin orbit interactions in the final state (as well as interchannel interactions between the 5s and 5p subshells). The small deviation in $\beta$ from the nonrelativistic value 2 that is obtained in this calculation is due to the weakness of the $^3P$ dipole amplitudes that are obtained. Comparison with the other calculations emphasizes the importance of using relativistic core wave functions when calculating forbidden dipole amplitudes. Similar $K$-matrix calculations for the photoelectron angular distribution of the 6s electron in Cs[69] were much more successful: $\beta$ was found to vary between +2 and –1, in agreement with experiment. In Cs, however, the deviation of $\beta$ from the nonrelativistic value 2 is due to interferences arising from a fine-structure splitting of an allowed dipole amplitude: $6s(^2S) \rightarrow \epsilon p(^2P_{3/2, 1/2})$. Thus in Cs a forbidden dipole amplitude does not have to be calculated, and treatment of only final state spin orbit interactions within a nonrelativistic set of basis functions appears not to be a bad approximation.
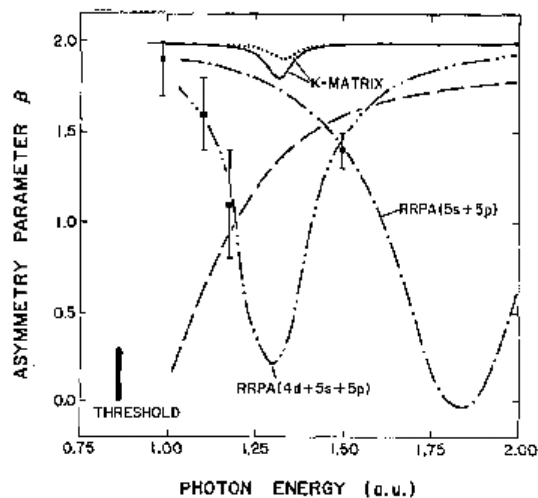


**Figure 14.** Photoelectron angular distribution asymmetry parameter $\beta$ for the 5s subshell in Xe: RRPA, relativistic RPA calculations of Johnson and Cheng[63] including interchannel correlations between the 5s + 5p and the 4d + 5s + 5p subshells; - - -, Dirac-Fock calculation of Ong and Manson[65]; $K$-matrix: calculations of Huang and Starace[68] including final-state spin orbit and 5s + 5p interchannel correlations in dipole length (·····) and velocity (——) approximation; ■, experimental results of White et al.[67]; ○, experimental result of Dehmer and Dill.[66]
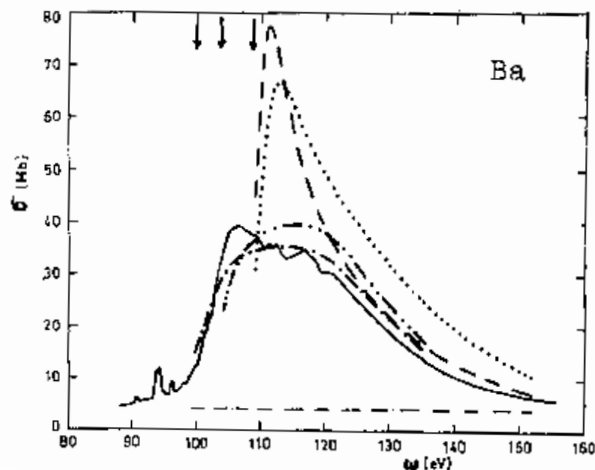
**Figure 15.** Photoionization cross sections for the $4d$ subshell of Ba. Experimental results of Rabe *et al.*[71]: ——. Theoretical results of Wendin[79]: ····· = intrachannel calculation; - - - = RPA; – ·· – = RPA + relaxation of $4d^{10}$, $5s^2$, and $5p^6$ subshells; – · – = RPA + relaxation of $4d^{10}$, $5s^2$, and $5p^6$ subshells + simulation of relativistic effects (from Reference 28).

## 2. Core Relaxation Effects

Whenever an electron is removed from an atom, the remaining electrons contract under the influence of the stronger net screened nuclear attraction. The deeper the subshell from which the electron is removed, the greater is the contraction of the outer subshell electrons. This contraction affects not only the ionic wave functions but also the binding energy and wave function of the photoelectron. One method of treating these effects is to use experimental binding energies and to employ ionic HF wave functions in the final state rather than keeping the atomic HF wave functions. Such a relaxed core approximation has been justified in the context of the RPA by Amusia.[70] In actuality, however, the importance of ionic relaxation depends on the energy of the photoelectron. When the photoelectron moves slowly, relaxation takes place while it is in the neighborhood, and hence there is a significant postcollision interaction with the core. This effect is not important at very high photoelectron escape velocities.

Wendin[28] has discussed relaxation from this more general point of view. In Figure 15 we show his results for the $4d$-subshell photoionization cross section in Ba. We see that relaxation effects reduce the unrelaxed RPA results by a factor of 2 and broaden them by a factor of 2! The final result, including relativistic interactions, is in very good agreement with experiment. [71]

Two final observations might be made: first, in the most general sense, relaxation effects include all processes by which an ion with a vacancy decays to a lower energy state. These processes include ejection of one or more Auger electrons and the emission of fluorescence radiation. When the photoelectron leaves the atom slowly, these relaxation processes should be considered together with the initial photoionization process. Second, we note that when one uses a correlated wave function to describe an atomic system, such as in

the hyperspherical coordinate description of He introduced by Macek,[58] relaxation effects are to a large extent taken care of since the wave function is a function of the relative positions of the electrons.

## 3. Long Range Polarization Fields

Polarization effects are known to cause difficulty in calculating photoionization cross sections for the alkalis and negative ions among others. We mention here, however, recent work of Greene *et al.*[72] on extending the quantum defect theory to treat an electron moving in any long range field. This work has already been used to give a detailed treatment of the polarization effects in photodetachment of negative ions near threshold.[73]

## C. Open-Shell Atoms

Except for the lightest atoms, relatively few open-shell atoms have been studied either experimentally or theoretically. On the one hand this is due to the experimental difficulty of producing open-shell atom vapors and on the other hand to the greater number of channels that must be considered in a theoretical calculation. Nevertheless a number of heavier open-shell atoms have been treated theoretically, among which are Al, Cl, and Ni. The $R$-matrix calculation of LeDourneuf *et al.*[74] for Al is shown in Figure 16. Excellent agreement is obtained with the measurements of Kohl and Parkinson[75] near threshold. Five theoretical calculations for Cl are shown in Figure 17; there is no available experimental measurement. Below $\hbar\omega = 22$ eV, all theoretical calculations except those of Starace and Armstrong[76] (which neglect interchannel coupling) agree; above $\hbar\omega = 22$ eV, there are significant unresolved discrepancies between open-shell RPA,[76, 77] MBPT,[78] and $R$-matrix[79] and close-coupling[80] calculations. The $R$-matrix calculations of Combet-Farnoux and Ben-Amar[81] for the $3d$ subshell of Ni represent a very ambitious detailed study of a rather complex atom.

A numerical difficulty in calculating open-shell atom cross sections is the large number of basis functions
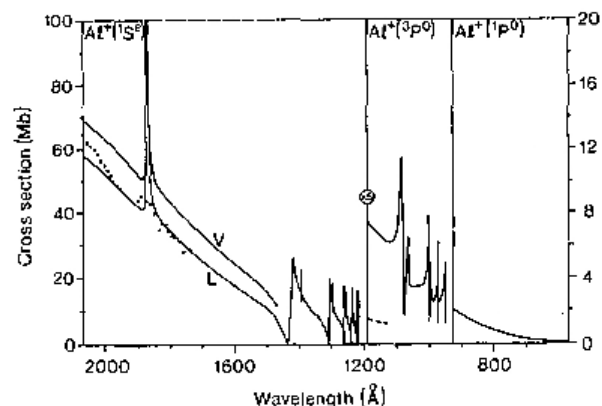


**Figure 16.** Photoionization cross section of aluminum: ——, $R$-matrix calculations of LeDourneuf *et al.*[74]; ·····, experimental data of Kohl and Parkinson.[75]
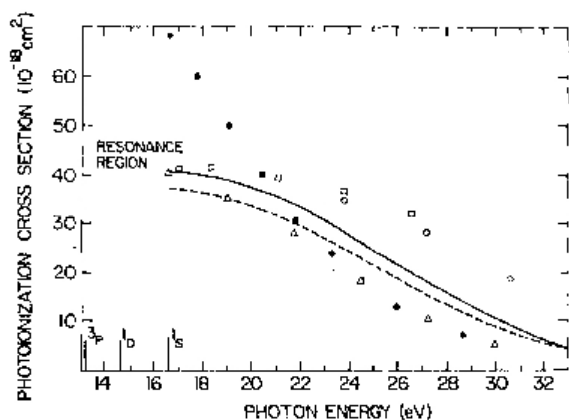
**Figure 17.** Calculated photoionization cross sections for the 3*p* subshell of atomic chlorine: ——, - - -, length and velocity MBPT calculations of Brown *et al.*[78]; □, close-coupling calculations of Conneely *et al.*[80]; ○, *R*-matrix calculations of Lamoureux and Combet-Farnoux[81]; ●, RPA calculations of Starace and Armstrong[76] (omitting interchannel interactions); △, RPA calculations of Cherepkov and Chernysheva.[77]

that must be used. In this connection, we note that Starace and Shahabi[82] have extended the transition matrix method of Chang and Fano[31] to treat an arbitrary open- or closed-shell atom in the RPA. A new graphical method for calculating the transition matrix was developed, which greatly simplifies the angular momentum algebra and provides a pictorial representation of the relevant interactions. To obtain dipole amplitudes one must solve a set of coupled differential equations at each photon energy for a limited number of initial and final correlated wave functions. These equations reduce to familiar forms in the following special cases: for closed-shell atoms the equations reduce to the Chang-Fano RPA equations[31]; in the absence of ground state correlations the equations reduce to the close-coupling equations.[83] Calculations for open-shell atoms are planned.[82]

## D. Photoionization of Atoms in External Fields

Photoionization of atoms in external uniform electric or magnetic fields leads to very interesting spectroscopic effects, among which are quasi-bound resonances in the continuum.[84, 85] Neither process is easy to treat theoretically, however. We sketch below the theoretical situations.

### 1. Uniform Magnetic Field

The Schrödinger equation for the hydrogen atom in a uniform magnetic field is not separable in any coordinate system. Near the origin, of course, electronic motion is best described in a spherical coordinate system, which is appropriate to the Coulomb attraction at $r = 0$. At large distances from the origin, electronic motion is best described in a cylindrical coordinate system, which is most appropriate for a uniform magnetic field. For low-energy excitations of the hydrogenic electron, the hydrogen atom has been found to be quasi-separable (in an adiabatic sense) in oblate spheroidal coordinates.[86] These coordinates reduce to spherical coordinates at the origin and in-

clude a substantial amount of magnetic field distortion at larger $r$. Near and above threshold, motion in the $Z = 0$ plane is bounded by the magnetic field. A 1-D WKB calculation of the bound energy levels[87] in this plane gives agreement with experimentally observed resonances.[84, 88] Development of a 2-D WKB solution for the wave function of these resonance states is being investigated.[89]

### 2. Uniform Electric Field

The Schrödinger equation for the hydrogen atom in a uniform electric field is separable in the parabolic coordinates $\xi$ and $\eta$. The motion in $\xi$ is always bounded, while the motion in $\eta$ is always unbounded, although there may be quasi-bound motion due to a potential barrier. Thus there are no rigorously bound states! For low excitations in H, one is concerned with the probability of field ionization.[90] For higher excitations, in the vicinity of threshold, a WKB calculation[91] of the bound energies for motion in the $\xi$ potential leads to energy level spacings that agree with experiment.[92]

For nonhydrogenic atoms the excited electron's motion is separable in parabolic coordinates only outside the atomic core. In a spherically symmetric coordinate system, which is appropriate near the origin, the excited electron's radial wave function is phase shifted with respect to a pure Coulomb wave by the atomic core. The matching of this phase-shifted spherical wave function onto the set of parabolic coordinate wave functions, which are more appropriate away from the origin, is a major task of theory.[93]

## References

1. U. Fano and J. W. Cooper, Rev. Mod. Phys. **40**, 441 (1968).
2. A. F. Starace, "Theory of Atomic Photoionization," in *Handbuch der Physik, Vol. 31*, W. Mehlhorn, Ed. (Springer, Berlin, 1980).
3. J. A. R. Samson, "Photoionization," in Reference 2.
4. D. J. Kennedy and S. T. Manson, Phys. Rev. A. **5**, 227 (1972).
5. J. W. Cooper, Phys. Rev. **128**, 681 (1962); see also Reference 1, Sec. 4.
6. F. Herman and S. Skillman, *Atomic Structure Calculations* (Prentice-Hall, Englewood Cliffs, N.J., 1963).
7. A. R. P. Rau and U. Fano, Phys. Rev. **167**, 7 (1968).
8. T. M. Zimkina, V. A. Fomichev, S. A. Gribovski, and I. I. Zhukova, Fiz. Tverd, Tela (Leningrad) **9**, 1447 (1967) [Sov. Phys. Solid State **9**,1128 (1967)]; V. A. Fomichev, T. M. Zimkina, S. A. Gribovski, and I. I. Zhukova, Fiz. Tverd, Tela (Leningrad) **9**, 1490 (1967) [Sov. Phys. Solid State **9**, 1128 (1967)]; R. Haensel, P. Rabe, and B. Sonntag, Solid State Commun. **8**, 1845 (1970); M. W. D. Mansfield and J. P. Connerade, Proc. R. Soc. London Ser. A: **352**, 125 (1976); H. W. Wolff, R. Bruhn, K. Radler, and B. Sonntag, Phys. Lett. A. **59**, 67 (1976); E.-R. Radtke, J. Phys. B. **12**, L71, L77 (1979).

9. B. Sonntag, R. Haensel, and C. Kunz, Solid State Commun. **7**, 597 (1969); J. P. Connerade, M. W. D. Mansfield, and M. A. P. Martin, Proc. R. Soc. London Ser. A: **350**, 405 (1976); R. Bruhn, B. Sonntag, and H. W. Wolff, Phys. Lett. A. **69**, 9 (1978); J. Phys. B. **12**, 203 (1979).

10. J. L. Dehmer, A. F. Starace, U. Fano, J. Sugar, and J. W. Cooper, Phys. Rev. Lett. **26**, 1521 (1971).

11. J. Sugar, Phys. Rev. B. **5**, 1785 (1972).

12. A. F. Starace, Phys. Rev. B. **5**, 1773 (1972); J. L. Dehmer and A. F. Starace, Phys. Rev. B. **5**, 1792 (1972); G. Wendin and A. F. Starace, J. Phys. B. **11**, 4119 (1978).

13. R. E. Dietz, E. G. McRae, Y. Yafet, and C. W. Caldwell, Phys. Rev. Lett. **33**, 1372 (1974); L. C. Davis and L. A. Feldkamp, Solid State Commun. **19**, 413 (1976).

14. J. Barth, F. Gerken, K. L. I. Kobayashi, J. H. Weaver, and B. Sonntag, J. Phys. C. **13**, 1369 (1980).

15. A. Msezane and S. T. Manson, Phys. Rev. Lett. **35**, 364 (1975).

16. A. F. Starace, Phys. Rev. A. **2**, 118 (1970).

17. J. A. R. Samson, Adv. At. Mol. Phys. **2**, 177 (1966).

18. L. Lipsky and J. W. Cooper (unpublished). Results presented in Figure 22 of Reference 1.

19. T. N. Chang, Phys. Rev. A. **15**, 2392 (1977).

20. H. P. Kelly and R. L. Simons, Phys. Rev. Lett. **30**, 529 (1973).

21. R. P. Madden, D. L. Ederer, and K. Codling, Phys. Rev. **177**, 136 (1969).

22. P. G. Burke and K. T. Taylor, J. Phys. B. **8**, 2620 (1975).

23. M. Ya. Amusia, V. K. Ivanov, N. A. Cherepkov, and L. V. Chernysheva, Phys. Lett. A. **40**, 361 (1972).

24. C. D. Lin, Phys. Rev. A. **9**, 181 (1974).

25. J. A. R. Samson and J. Gardner, Phys. Rev. Lett. **33**, 671 (1974).

26. R. G. Houlgate, J. B. West, K. Codling, and G. V. Marr, J. Electron Spectrosc. Relat. Phenom. **9**, 205 (1976).

27. M. Ya. Amusia and N. A. Cherepkov, Case Stud. At. Phys. **5**, 47 (1975).

28. G. Wendin, in *Photoionization and Other Probes of Many- Electron Interactions,* F. J. Wuilleumier, Ed. (Plenum, New York, 1976), pp. 61-82.

29. H. P. Kelly, in *Photoionization and Other Probes of Many- Electron Interactions,* F. J. Wuilleumier, Ed. (Plenum, New York, 1976), pp. 83-110.

30. P. G. Burke and W. D. Robb, Adv. At. Mol. Phys. **11**, 143 (1975).

31. T. N. Chang and U. Fano, Phys. Rev. A. **13**, 263, 282 (1976).

32. J. R. Swanson and L. Armstrong, Jr., Phys. Rev. A. **15**, 661 (1977); **16**, 1117 (1977).

33. U. Fano, Phys. Rev. **124**, 1866 (1961).

34. A. F. Starace, Phys. Rev. A. **16**, 231 (1977).

35. N. M. Kabachnik and I. P. Sazhina, J. Phys. B. **9**, 1681 (1976).

36. M. J. Seaton, Mon. Not. R. Astron. Soc. **118**, 504 (1958); Proc. Phys. Soc. **88**, 801, 815 (1966).

37. K. T. Lu and U. Fano, Phys. Rev. A. **2**, 81 (1970); U. Fano, Phys. Rev. A. 2,353 (1970); **15**, 817 (1977); K. T. Lu, Phys. Rev. A. **4**, 579 (1971).

38. U. Fano and C. M. Lee, Phys. Rev. Lett. **31**, 1573 (1973); C. M. Lee, Phys. Rev. A. **10**, 584 (1974).

39. J. Dubau and J. Wells, J. Phys. B. **6**, 1452 (1973).

40. A. I. Baz, Zh. Eksp. Teor. Fiz. **36**, 1762 (1959) [Sov. Phys. JETP 9, 1256 (1959)].

41. M. Gailitis, Zh. Eksp. Teor. Fiz. **44**, 1974 (1963) [Sov. Phys. JETP 17, 1328 (1963)1.

42. P. L. Altick, Phys. Rev. A. **21**, 1381 (1980).

43. V. Schmidt, N. Sandner, H. Kuntzemüller, P. Dhez, F.Wuilleumier, and E. Kallne, Phys. Rev. A. **13**, 1748 (1976); G. R. Wight and M. J. Van der Wiel, J. Phys. B. **9**, 1319 (1976).

44. F. W. Byron and C. J. Joachain, Phys. Rev. **164**, 1 (1967).

45. R. L. Brown, Phys. Rev. A. **1**, 586 (1970).

46. T. N. Chang, T. Ishihara, and R. T. Poe, Phys. Rev. Lett. **27**, 838 (1971).

47. T. A. Carlson, Phys. Rev. **156**, 142 (1967).

48. T. N. Chang and R. T. Poe, Phys. Rev. A. **12**, 1432 (1975).

49. J. A. R. Samson and G. N. Haddad, Phys. Rev. Lett. **33**, 875 (1974).

50. S. L. Carter and H. P. Kelly, Phys. Rev. A. **16**, 1525 (1977).

51. S. L. Carter and H. P. Kelly, J. Phys. B. **9**, L565 (1976).

52. S. L. Carter and H. P. Kelly, J. Phys. B. **9**, 1887 (1976).

53. T. Aberg, in *Photoionization and Other Probes of Many-Electron Interaction,* F. Wuilleumier, Ed. (Plenum, New York, 1976), pp. 49-59.

54. A. Niehaus, J. Phys. B. **10**, 1845 (1977).

55. V. L. Jacobs and P. G. Burke, J. Phys. B. **4**, L67 (1972); H. A. Hyman, V. L. Jacobs, and P. G. Burke, J. Phys. B. **5**, 2282 (1972).

56. F. Wuilleumier, M. Y. Adam, N. Sandner, and V. Schmidt, J. Phys. (Paris) Lett **41**, L373 (1980).

57. J. W. Cooper, U. Fano, and F. Prats, Phys. Rev. Lett. **10**, 518 (1963).

58. J. Macek, J. Phys. B. **1**, 831 (1968).

59. D. L. Miller and A. F. Starace, J. Phys. B **13**, L525 (1980).

60. J. A. R. Samson, Phys. Rep. **28C**, 303 (1976).

61. C. Greene, Phys. Rev. A. (in press).

62. W. R. Johnson and C. D. Lin, Phys. Rev. A. **20**, 964 (1979).

63. W. R. Johnson and K. T. Cheng, Phys. Rev. A. **20**, 978 (1979).

64. K.-N. Huang, W. R. Johnson, and K. T. Cheng, Phys. Rev. Lett. **43**, 1658 (1979).

65. W. Ong and S. T. Manson, J. Phys. B **11**, L65 (1978); Phys. Rev. A. **19**, 688 (1979).

66. J. L. Dehmer and D. Dill, Phys. Rev. Lett. **37**, 1049 (1976).

67. M. G. White, S. H. Southworth, P. Kobrin, E. D. Poliakoff, R. A. Rosenberg, and D. A. Shirley, Phys. Rev. Lett. **43**, 1661 (1979).

68. K.-N. Huang and A. F. Starace, Phys. Rev. A. **21**, 697 (1980).

69. K.-N. Huang and A. F. Starace, Phys. Rev. A. **19**, 2335 (1979).

70. M. Ya. Amusia, in *Atomic Physics, Vol. 5,* R. Marrus, M. Prior, and H. Shugart, Eds. (Plenum, New York, 1977), p. 537.

71. P. Rabe, K. Radler, and H. W. Wolff, *Vacuum Ultraviolet Radiation Physics,* E. E. Koch, R. Haensel, and C. Kunz, Eds. (Pergamon-Vieweg, Braunschweig, 1974), p. 247.

72. C. H. Greene, U. Fano, and G. Strinati, Phys. Rev. A. **19**, 1485 (1979); C. Greene, Phys. Rev. A. **22**, 149 (1980).

73. C. H. Greene, J. Phys. B. **13**, L39 (1980); S. Watanabe and C. H. Greene, Phys. Rev. A. **22**, 158 (1980).

74. M. LeDourneuf, V. K. Lan, P. G. Burke, and K. T. Taylor, J. Phys. B. **8**, 2640 (1975).

75. J. L. Kohl and W. H. Parkinson, Astrophys. J. **184**, 641 (1973).

76. A. F. Starace and L. Armstrong, Jr., Phys. Rev. A. **13**, 1850 (1976).

77. N. A. Cherepkov and L. V. Chernysheva, Phys. Lett. A. **60**, 103 (1977).

78. E. R. Brown, S. L. Carter, and H. P. Kelly, Phys. Rev. A. **21**, 1237 (1980).

79. M. Lamoureux and F. Combet-Farnoux, J. Phys. (Paris) **40**, 545 (1979).

80. M. J. Conneely, K. Smith, and L. Lipsky, J. Phys. B. **3**, 493 (1970).

81. F. Combet-Farnoux and M. Ben-Amar, Phys. Rev. A. **21**, 1975 (1980).

82. A. F. Starace and S. Shahabi, Phys. Scr. **21**, 368 (1980).

83. K. Smith, R. J. W. Henry, and P. G. Burke, Phys. Rev. **147**, 21 (1966).

84. For resonances in a uniform magnetic field, see W. R. S. Garton and F. S. Tomkins, Astrophys. J. **158**, 839 (1969).

85. For resonances in a uniform electric field, see R. R. Freeman, N. P. Economou, G. C. Bjorklund, and K. T. Lu, Phys. Rev. Lett. **41**, 1463 (1978).

86. A. F. Starace and G. L. Webster, Phys. Rev. A. **19**, 1629 (1979).

87. A. F. Starace, J. Phys. B. **6**, 585 (1973).

88. R. J. Fonck, D. H. Tracy, D. C. Wright, and F. S. Tomkins, Phys. Rev. Lett **40**, 1367 (1978).

89. U. Fano, Phys. Rev. A. (in press).

90. See, e.g., T. Yamabe, A. Tachibana, and H. J. Silverstone, Phys. Rev. A. **16**, 877 (1977).

91. A. R. P. Rau, J. Phys. B. **12**, L193 (1979).

92. R. R. Freeman and N. P. Economou, Phys. Rev. A. **20**, 2356 (1979).

93. U. Fano, Colloq. Int. CNRS **273**, 127 (1977).